IEEE Access
Multidisciplinary ⋮ Rapid Review ⋮ Open Access Journal

Received 25 March 2023, accepted 7 April 2023, date of publication 11 April 2023, date of current version 14 April 2023.

Digital Object Identifier 10.1109/ACCESS.2023.3266240

RESEARCH ARTICLE

Mitigation of Temperature Effects and Performance Enhancement of Perovskite Solar Cells Using Nano-Pyramids Grating

ALAA A. ZAKY[1], SHOROK ELEWA[1], SALEH ALYAHYA[2], (Member, IEEE), MUJAHED AL-DHAIFALLAH[3,4], (Member, IEEE), HEGAZY REZK[5], AND BEDIR YOUSIF[1,2], (Member, IEEE)

[1]Electrical Engineering Department, Kafrelsheikh University, Kafrelsheikh 33511, Egypt
[2]Electrical Engineering Department, Faculty of Engineering and Information Technology, Onaizah Colleges, Al Qassim 51911, Saudi Arabia
[3]Control and Instrumentation Engineering Department, King Fahd University of Petroleum and Minerals, Dhahran 31261, Saudi Arabia
[4]Interdisciplinary Research Center (IRC) for Renewable Energy and Power Systems, King Fahd University of Petroleum and Minerals, Dhahran 31261, Saudi Arabia
[5]Department of Electrical Engineering, College of Engineering in Wadi Alddawasir, Prince Sattam bin Abdulaziz University, Al-Kharj 11942, Saudi Arabia

Corresponding author: Mujahed Al-Dhaifallah (mujahed@kfupm.edu.sa)

This work was supported by Prince Sattam bin Abdulaziz University under Project PSAU/2023/R/1444.

ABSTRACT For their impressive electrical and optical characteristics, perovskite solar cells (PSCs) have been presented to the nanostructured photovoltaics field as one of the encouraging replacements of both conventional silicon based solar cells (SCs) and thin film SCs. In this paper, we present a study of the performance of $CH_3NH_3PbI_3$ PSC, as one of the prime candidates of PSCs, at different values of temperature and solar irradiance power with the aid of a 3-D finite element method (FEM) COMSOL Multiphysics simulation indicating the significant reduction of the PSC's power conversion efficiency (PCE) upon either increasing the operating temperature or decreasing solar irradiance power. Then, we study the effect of electron transporting layer (ETL) grating on the electrical parameter of the cell. Results of the proposed study show that for PSCs with optimal 400nm $CH_3NH_3PbI_3$ absorber thickness and adjusted thickness of other layers, adding pyramid grating to ETL causes the power conversion efficiency (PCE) to go up to 21.058% instead of 19.818% in case of flat layer at room temperature, with short circuit current density (J_{SC}) of 25.858mA/cm^2, open circuit voltage (V_{OC}) of 1Volt and 81.44% filling factor (FF). Results also indicate that using such periodic structure of ETL can compensate the reduction of PCE caused by temperature increasing.

INDEX TERMS Nanograting, layer thickness, PCE, perovskite, solar cells.

I. INTRODUCTION

Following the same operating mechanism as the ordinary Dye sensitized solar cells (DSSCs) with their four main steps of operation, absorption of light, injection of carriers into transport layers, carriers' transportation and then electrodes collection of current, perovskite solar cells (PSCs) have succeeded to achieve even higher power conversion efficiency (PCE) than that of DSSCs by replacing the main light absorber material by perovskite [1]. Recently, PSCs attract great attention of photovoltaic scientists and researchers as they have impressive industrial characteristics such as low cost of production, perfect flexible and thin structure [2], [3], they also have outstanding optoelectronic characteristics that may be employed to achieve higher performance and acceptable PCE. Having a light absorber material with variable bandgaps, long carriers' diffusion length, carrier mobilities of moderated values in addition to their high absorption coefficient values [4], [5], [6], PSCs' efficiency jumps from its first tested value of 3.8% [7] up to 25.6% [8] over the last decade.

Based on availability and cost effectiveness, methylammonium lead halide material is considered the most common

The associate editor coordinating the review of this manuscript and approving it for publication was Mauro Gaggero.

material utilized in PSCs as main absorber. methylammonium lead halide material can be considered as a hybrid between organic and inorganic materials that has the crystal structure order of ABX_3 [3]. Materials such as $CH_3NH_3PbI_3$ have shown a great potential to be active absorptive materials used in the PSC [9], [10], [11], [12], yet with some environmental considerations of using such materials containing harmful heavy metal cations [13], [14], [15]. While the most effective light trapping techniques listed as follows: plasmonic nanostructures [16], [17], [18], periodic and random scattering surfaces [19], [20], [21], [22], [23], nanowires [24], [25], [26] and photonic crystal structures [27], [28], [29] are usually used to enhance the performance of solar cells, they also can be considered one of the most suitable solutions for reducing the toxicity of PSCs [30], [31]. The amount of toxic cation can be reduced by shortening the perovskite absorber, leading to reduction in the optical path length and in turn to reduction in the photogenerated current. Yet, the utilizing of light trapping techniques compensates that reduction of photocurrent based on increasing the absorption of PSCs [19], [32], [33].

PSCs' performance parameters (i.e., short circuit current density (J_{SC}), open circuit voltage (V_{OC}), PCE, filling factor (FF)), get affected with the variation of operation parameters, specially, the variation of temperature and cells' layers thickness [34].

This paper, proposes a pyramid shape grating for 3rd generation perovskite solar cells electron transporting layer to enhance their performance which did not discussed previously up to the knowledge of the authors. Moreover, investigating the behavior of 3rd generation perovskite solar cells under the effect of changing the device layers thickness and at different values of temperature and solar irradiance power via a 3-D finite element method (FEM) COMSOL Multiphysics simulation.

In this research paper, we introduce COMSOL Multiphysics simulation of PSCs in 3D geometry, studying both off its optical and electrical characteristics, then the thickness changing effect of cell's layers on its performance parameters investigated numerically, also the effect of temperature variation between 25°C and 80°C and sun power changing on the performance of the PSCs has been examined. Finally, the effect of changing the ETL geometric structure to different shapes on the PCE of PSCs also investigated.

This work is structured as follows: section II illustrates the proposed PSCs modeling and the parameters used in simulation process; it also mentions the equations that govern the operation of PSCs. The simulation results of the proposed PSCs using finite element method (FEM) are presented in section III. Finally, section IV concludes the main conclusions.

II. MODELING AND STRUCTURE

A. PSCs STRUCTURE AND MATERIALS

The optical and electrical performance of PSC having the thin film structure presented in literature [35] is investigated and analyzed based on COMSOL Multiphysics software, we studied, only with changing the metallic contact to be silver instead of gold. Consisting of five layers, Fig. 1(a) indicates the proposed structure of PSC ordered up to bottom as follows: transparent conducting front contact made of fluorine doped tin oxide (FTO), n-doped layer of TiO_2 as electron transportation layer (ETL), p-doped absorber layer made of $CH_3NH3PbI3$ perovskite, p-doped Spiro-MeOTAD layer as hole transportation layer (HTL) and the silver back reflector metallic contact layer. For the purpose of achieving accurate optical simulation, an air layer at the cell surface was added.

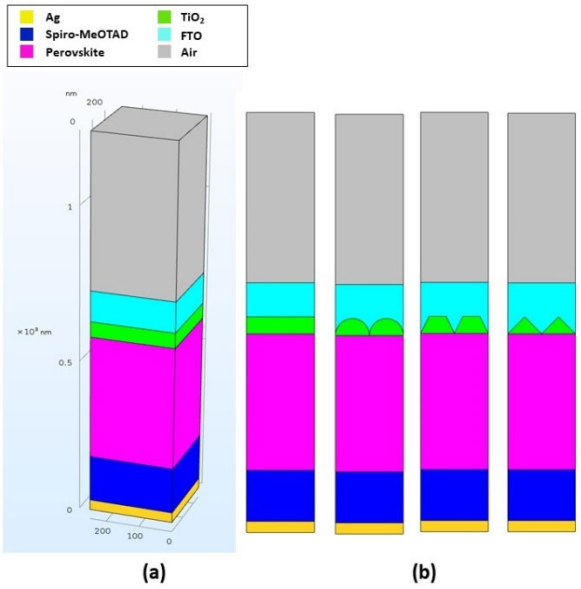

FIGURE 1. (a) Planar PSCs construction; (b) 2D cross section view PSC with different ETL geometric structure.

TABLE 1. Proposed PSCs parameters.

Parameters	Spiro-MeOTAD	$CH_3NH_3PbI_3$	TiO_2	FTO
Thickness ***(nm)***	350 (variable)	330 (variable)	50(variable)	100 (variable)
ε_r	3 [38]	6.5 [36]	9 [36]	9 [37]
N_c (cm^{-3})	10^{20} [38]	$1.66 * 10^{19}$ [36]	10^{19} [36]	$2.2 * 10^{18}$ [37]
N_v (cm^{-3})	10^{20}[38]	$5.41 * 10^{19}$ [36]	10^{19} [36]	$1.8 * 10^{19}$ [37]
μ_n / μ_p (cm^2/Vs)	2/0.1 [38]	50/50 [36]	20/10 [36]	20/10 [37]
E_g (eV)	3 [38]	1.55 [36]	3.2 [36]	3.5 [37]
χ (eV)	2.45 [38]	3.93 [36]	4 [36]	4 [37]
N_A (cm^{-3})	$2 * 10^{18}$ [35]	$3 * 10^{15}$ [35]	-	-
N_D (cm^{-3})	-	-	$5 * 10^{18}$ [35]	$2 * 10^{19}$ [35]
τ_n / τ_p (ns)	0.1/0.1 [35]		8/8 [35]	5/2 [35]

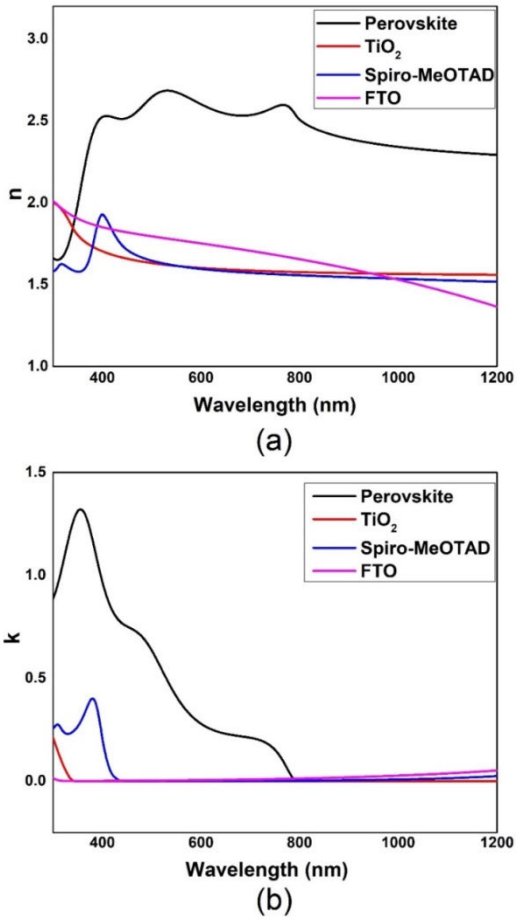

FIGURE 2. Refractive indices (a) The real and (b) imaginary part for FTO, TiO_2, $CH_3NH_3PbI_3$ perovskite, and Spiro-MeOTAD.

All the optical and electrical parameters of the mentioned materials were taken from relevant studies [35], [36], [37], [38], and utilized to simulation by either using the material library of COMSOL or adding manually to the structure. Table 1 indicates the main parameters of PSC, where ε_r is the dielectric constant of the material, N_c and N_v are the conduction and valence bands effective concentration of states, correspondingly, μ_n and μ_p are the mobilities of electrons and holes, correspondingly, N_A and N_D are the doping density of acceptor and donor atoms, respectively, τ_n and τ_p are the life time of electrons and holes, correspondingly.

Fig. 2(a) and Fig. 2(b) indicate the real and the imaginary parts of refractive indices of each layer of PSC structure mentioned in relevant literatures [39], [40], we utilized this data in form of interpolation function depending on the light wavelength and imported them to material optical parameters of our simulation.

The values of bandgap energy (E_g) mentioned in Table 1 is the effective energy gap of the materials at room temperature, yet, the effect of temperature varying on the energy gap values was taken into consideration by extracting published data from relevant literatures [41], [42], [43], and adding them as interpolation functions of temperature then imported to material parameters.

B. PHYSICS

To determine the PSCs optical and electrical characteristics, we used FEM based study using RF and semiconductor COMSOL modules. At first, the simulation was computed with the parameters declared in Table 1, then recomputed at changed temperature values and different thickness of absorber and transporting layers.

For the optical study, the input solar power applied to the top side of the cell was added using the standard AM1.5G values as a plane wave with interpolated function depending on the incident light wavelength. The boundary conditions of Floquet were added to each two facing sides of the structure to form a unit cell with equal width and depth that can be duplicated in both vertical directions to reduce the computation time.

To determine the value of electric field through the different layers of PSCs, the wave equation of Helmholtz's derived from frequency domain Maxwell's equation was solved [38]:

$$\nabla \times (\nabla \times E) - k_0^2 \varepsilon_r E = 0 \tag{1}$$

where, E, k_0 and ε_r are electric field, the wave number and the dielectric constant of material. Relative permittivity of materials depends on the refractive index value, then it may be considered as function of incident light wavelength as follows [38]:

$$\varepsilon_r = \varepsilon' + j\varepsilon'' = (n(\lambda) - jk(\lambda))^2 \tag{2}$$

where n and k as functions of wavelength are shown in Fig. 2, ε' and ε'' are the real and imaginary parts of relative permittivity, respectively.

The carriers generating rate can be calculated using the electric field inside each layer as follows [36]:

$$G_{ph}(\lambda) = \varepsilon'' |E|^2 / 2\hbar \tag{3}$$

where, $\hbar$ is reduced Plank's constant.

The generation rate of electrons and holes can be calculated over selected range of wavelength as follows [36]:

$$G_{tot} = G_n = G_p = \int_{\lambda_{min}}^{\lambda_{max}} G_{ph}(\lambda)\, d\lambda \tag{4}$$

where, G_n and G_p are the generation rates of electrons and holes, correspondingly, $\lambda_{min} - \lambda_{max} = 300 - 1000$nm.

SC's absorption can be calculated using the S-parameters as follows [36]:

$$\text{Absorption} = 1 - |S_{11}|^2 - |S_{21}|^2 \tag{5}$$

where, $|S_{11}|^2$ is transmission and $|S_{21}|^2$ is reflection.

For the semiconductor electrical study, Poisson's and continuity equations have been solved using semiconductor

COMSOL module to determine the short circuit current density and open circuit voltage of PSCs as follows [36]:

$$\nabla.(\varepsilon_0\varepsilon_r\nabla\varphi) = -\rho \tag{6}$$

$$\frac{\partial n}{\partial t} = \frac{1}{q}\nabla J_n + G_n - R_n \tag{7}$$

$$\frac{\partial p}{\partial t} = \frac{1}{q}\nabla J_p + G_p - R_p \tag{8}$$

where ε_0 is permittivity of vacuum, φ is electrostatic potential, q is electron charge and ρ is charge density determined as follows [36]:

$$\rho = q(n - p - N_D + N_A) \tag{9}$$

where n and p are the electron and hole concentrations, respectively. Holes and electrons generation rates (G_p and G_n), are determined using the previously mentioned optical investigation, while carriers recombination rates (R_n and R_p) can be calculated with the aid of Shockley Rear Hall trapping model as follows [4]:

$$R = (np - n_i^2) \Big/ (\tau_n (n + n_i) + \tau_p (p + n_i)) \tag{10}$$

An ideal ohmic contact was selected to express FTO front contact, on the other side, the silver back contact was selected to be Schottky's contact. The surface velocity of recombination is 10^7cm/s for both electrons and holes.

With the aid of drift diffusion model, current densities of electrons and holes is determined as follows [36]:

$$J_n = -q\mu_n n\nabla\varphi + qD_n\nabla n \tag{11}$$

$$J_p = -q\mu_p p\nabla\varphi - qD_p\nabla p \tag{12}$$

To study the temperature effect on PSCs electrical performance, the amount of changing in intrinsic carrier density was taken into consideration as it depends on temperature as follows:

$$n_i = \sqrt{N_c N_v}\, e^{-E_g(T)/KT} \tag{13}$$

where n_i, N_c, N_v, E_g, K and T are the intrinsic carriers' concentrations, effective density of states for conduction and valence bands, energy band gap, Boltzmann's constant and temperature, respectively.

Although, carrier mobilities of semiconductor materials are temperature dependent parameters, (Xia et al.) has experimentally and mathematically proved that for temperatures above 300K, the lead-halide perovskite carriers' mobilities are almost constant [44]. Then the change of carriers mobilities caused by temperature variation can be neglected over the chosen range of temperature in this study.

III. RESULTS AND DISCUSSIONS

A. EFFECT OF CHANGING LAYERS' THICKNESS

The effect of changing the FTO glass layer thickness on the PSCs performance is presented in Fig. 3, the thickness of the FTO was varied between 100 – 900nm with observed decrease of 6.2% in PCE and almost a constant value of FF. The drop of PCE is mainly because of the decreasing of

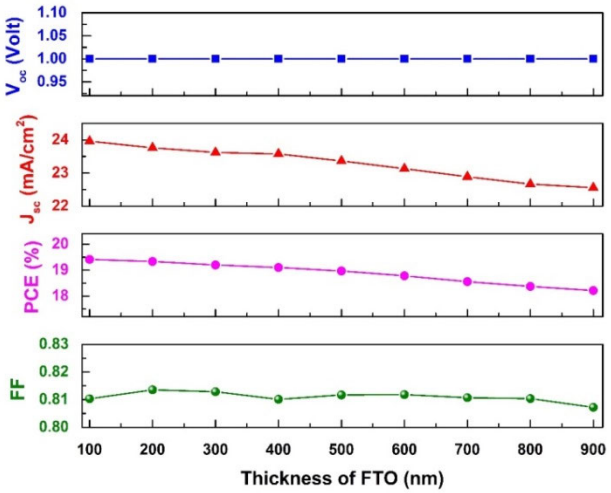

FIGURE 3. PSC's parameters variation depending on the FTO layer thickness.

J_{SC} value from 23.96 mA/cm^2 to 22.56 mA/cm^2, while the value of V_{OC} remains unchanged with FTO layer thickness variation.

Increasing FTO thickness leads to increasing that sheet resistance, causing the series resistance of PSC to be higher and that in turn reduce J_{SC}; also, from the optical study perspective, increasing the FTO thickness lowers the amount of light radiation reaching to the main absorber layer which causes reduction in carrier generating rates and in turn reduces the value of J_{SC}. As the thickness of FTO does not have any effect on the energy levels, thus the value of V_{OC} remains unchanged.

The effect of varying $CH_3NH_3PbI_3$ perovskite layer thickness between 100 – 1000nm on the PSCs performance parameters is displayed in Fig. 4 Changing the main absorber thickness affects both J_{SC} and V_{OC}, which in turn affects the FF and PCE values.

Increasing the absorber thickness causes increasing in JSC as a result of increasing the optical track length of light inside the cell which increase the absorption of the cell and in turn the current density. On the other hand, increasing the absorber thickness beyond the carrier's diffusion length causes rising in the charge recombination rates and that leads to reduction of V_{OC} value. For PSC with parameters mentioned in Table 1, max PCE was found to be 19.69% with absorber thickness of 400nm, J_{SC} of 24.42mA/cm^2, V_{OC} of 1V,and FF of 80.7%.

In this research, HTL was selected to be Spiro-MeOTAD material for its impressive performance with PSCs [45]. Fig. 5 indicated the effect of Spiro-MeOTAD layer thickness variation on the performance of the PSC over HTL thickness variation between 100 – 1050nm. The PCE maximum and minimum values over the variation range were 19.61% and 18.78% for Spiro-MeOTAD thickness of 150nm and 1050nm respectively.

The value of V_{OC} was not affected by the HTL thickness variation, yet, the value of J_{SC} changed as a result of changing

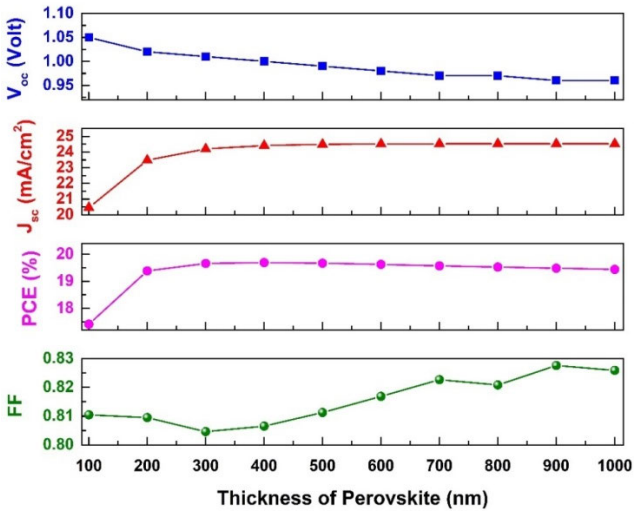

FIGURE 4. PSC's parameters variation depending on the perovskite absorber layer thickness.

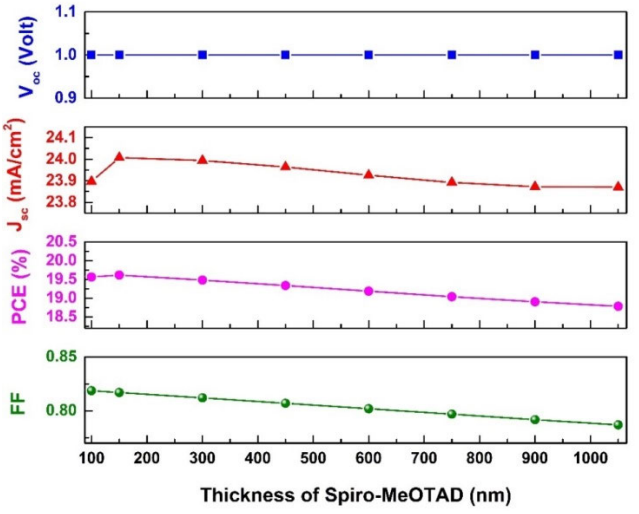

FIGURE 5. PSC's parameters variation depending on the Spiro-MeOTAD HTL thickness.

the ability of this layer to transport carriers to the external contact which depends on the carriers' diffusion length. The total change of J_{SC} value caused by changing HTL thickness with the mentioned variation range was found to be 0.574%. That negligible variation in PCE and J_{SC} values is an evident that the Spiro-MeOTAD HTL does not interfere in the optics of the PSC.

It has been proved that the finest performance of PSCs is accomplished using TiO_2 as ETL [45]. The effect of changing the thickness of TiO2 layer on the PSCs parameters is presented in Fig. 6, the thickness of the TiO_2 layer was varied between $50 - 520$nm with observed reduction of 0.224% in PCE and almost a constant value of FF.

The drop of PCE is mainly because of the decreasing of J_{SC} value, while the value of $_{VOC}$ remains unchanged with TiO_2

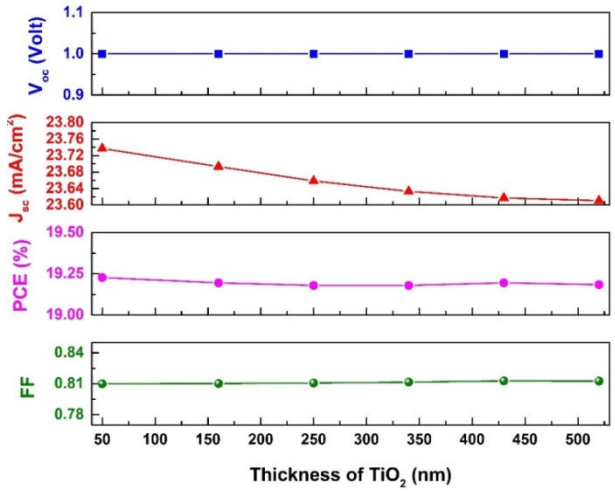

FIGURE 6. PSC's parameters variation depending on the TiO_2 ETL thickness.

layer thickness variation. These results can be interpreted as the thickness of TiO_2 layer increases, the electrons' diffusion length and mobility decrease in the ETL due to the increasing of charge trap defects in the TiO_2 thicker layer which in turn results in short circuit current density reduction.

From the previously mentioned results in Fig. 3- Fig. 6, it can be concluded that the optimized thickness of each layer of PSC in our study are 400nm for the main $CH_3NH_3PbI_3$ absorber, 50nm for the TiO_2 ETL, 150nm for the Spiro-MeOTAD HTL and 100nm for the FTO layer.

With these optimized dimensions of each layer, the optical and electrical studies were repeated at room temperature. The electrical parameters in this case were found to be as follows: $J_{SC}= 24.3658 mA/cm^2$, $V_{OC}= 1$Volt, FF = 82.2% and PCE = 19.818%.

B. EFFECT OF CHANGING TEMPERATURE

Just as any other types of solar cells, operating temperature has a great influence on the overall performance of PSCs. The effect of temperature variation on the PSCs parameters is shown in Fig. 7 over $25 - 80°C$ temperature change range.

As indicated in this figure, temperature variation mainly affects the V_{OC} not the Jsc. The reduction of V_{OC} value with increasing temperature results from the increasing of carriers' recombination probabilities while the carriers photogeneration rates extracted from the optical study are almost the same at different temperature values, therefore, the value of J_{SC} is approximately constant. Also, from the electrical study perspective, changing the temperature affects the bandgap energy of the absorber, increasing the temperature leads to reduction of bandgap energy of the active absorber that means that less energy is needed to extract carriers from device terminals and then lower value of V_{OC}.

When the temperature raised from 25°C to 80°C, about 2.722% drop in PCE was observed caused by changing V_{OC} between 1V and 0.89V and FF of 81.7% and 79.2%

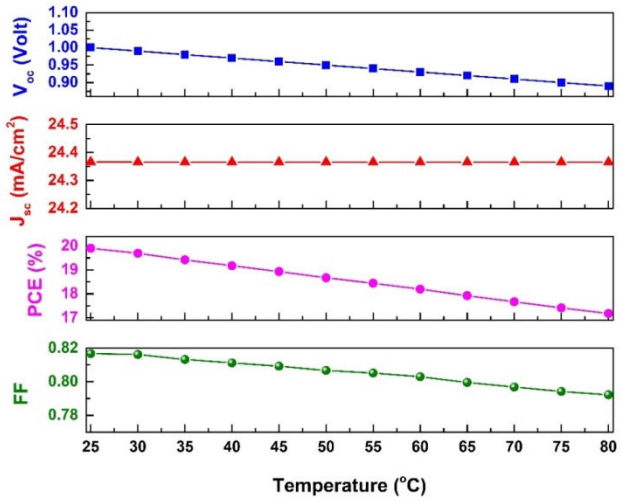

FIGURE 7. PSCs parameters variation depending on temperature.

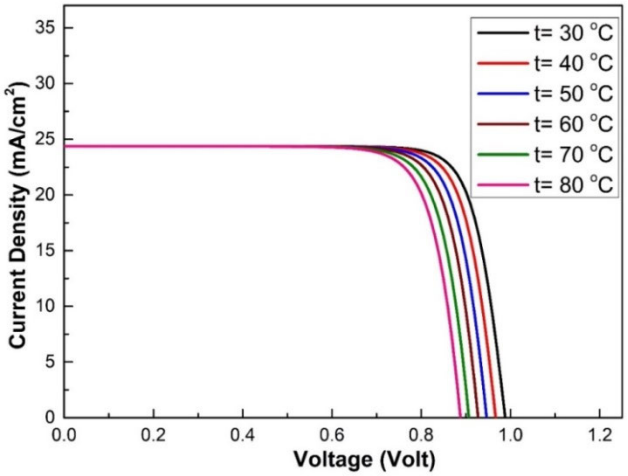

FIGURE 8. JV curves of proposed PSC at different values of temperature.

respectively. The JV curves at different values of temperature shown in Fig. 8 indicate same results previously mentioned in Fig. 7 only with 10°C variation step to make it easier to recognize the variation in V_{OC} value caused by temperature changing.

Fig. 9 and Fig. 10 show the effect of changing temperature on both electrons and holes densities across the PSC layers after taking the common logarithm to indicate the variation range of both electrons and holes concentrations. Both figures indicate the expected result that electron density decreases gradually from its highest value at the top of the FTO contact to its lowest value at the bottom of HTL, on the other side, the density of holes is at its peak value at bottom edge of the HTL and minimum value at the front side of FTO contact. While the temperature variation may have slight effect on carrier concentration, yet, these two figures indicate more obvious variation in the electrons concentration than the holes concentration can be caused by temperature alternating, that

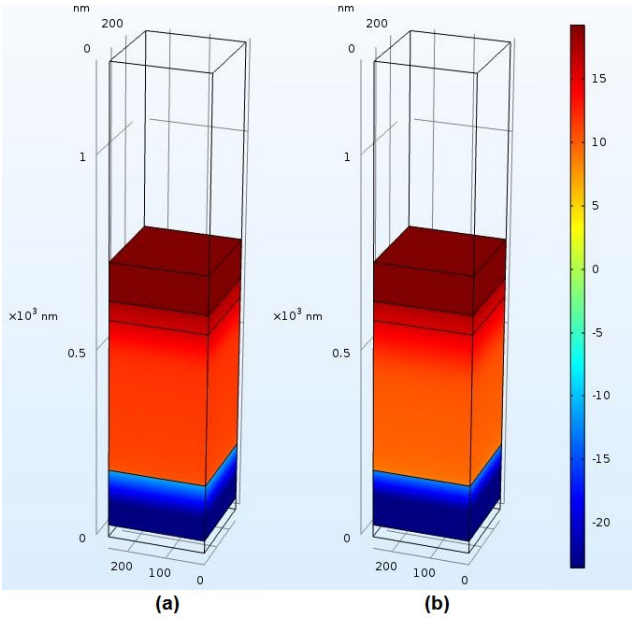

FIGURE 9. Electron density across the PCS at (a) 25°C (b) 80°C.

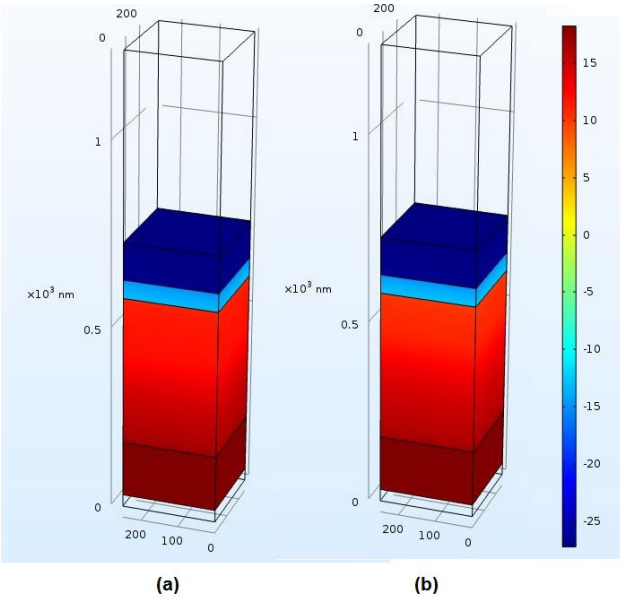

FIGURE 10. Holes density across the PCS at (a) 25°C (b) 80°C.

can be interpreted by the fact that the temperature value has significant influence on the minority carrier density, in our case the electrons in the P-type absorber, than the majority carrier density.

C. EFFECT OF CHANGING SUN IRRADIANCE

The influence of varying the sun irradiance on the PSCs JV curve is indicated in Fig. 11 and Fig. 12, keeping temperature unchanged at 30°C and under solar irradiance of 1sun (1000W/m^2), 0.7 sun (700W/m^2), 0.5 sun(500W/m^2), 0.3 *sun*(300W/m^2) and 0.1*sun* (100W/m^2), J_{SC} values were

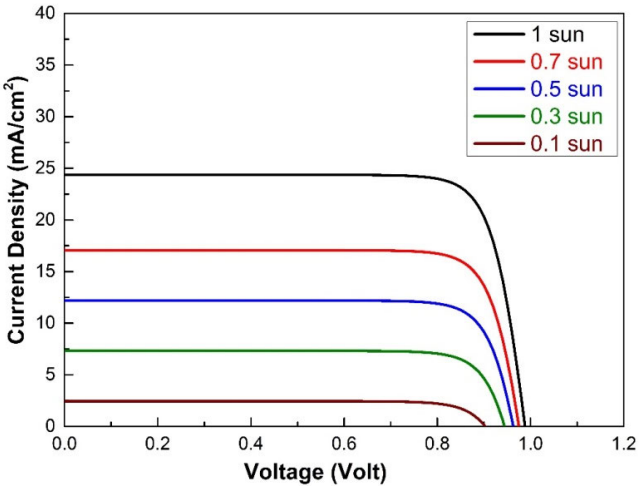

FIGURE 11. JV curves of PSC under variable solar irradiance.

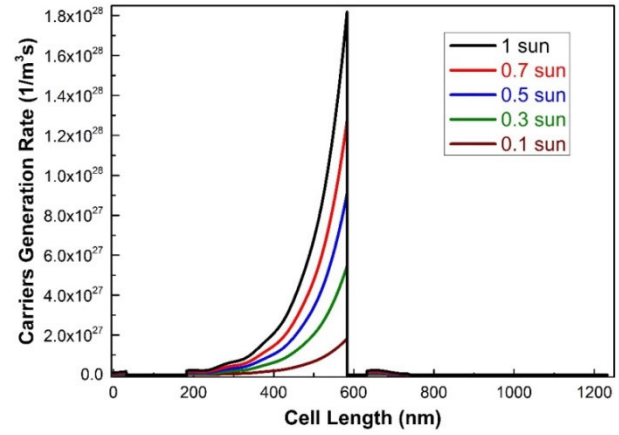

FIGURE 12. Carriers generation rate profile for PSC under variable solar irradiance.

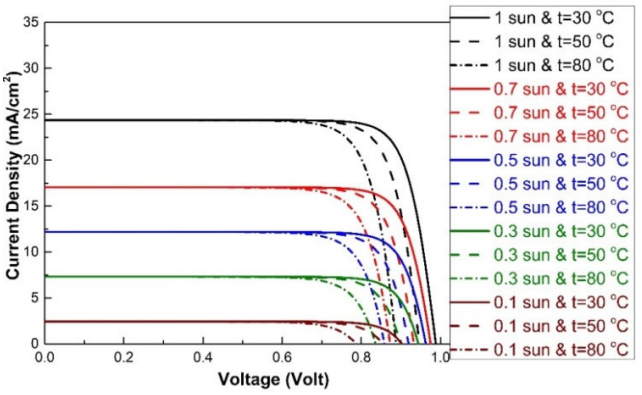

FIGURE 13. JV curves of PSC at different values of solar irradiance and temperature.

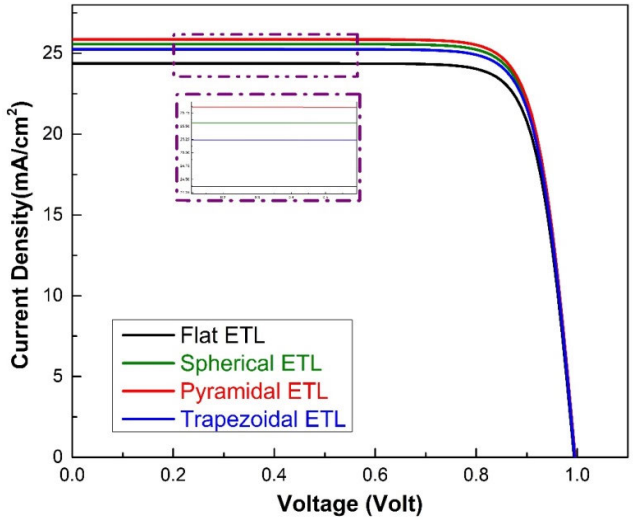

FIGURE 14. JV curves of the proposed PSC with different ETL geometric structure.

found to be 24.366mA/cm^2, 17.06mA/cm^2, 12.18mA/cm^2, 7.3mA/cm^2 and 2.44mA/cm^2 respectively.

The values of V_{OC} over the same solar irradiance values were 0.99V, 0.98V, 0.96V, 0.94V and 0.9V with coresponding PCE of 19.69%, 19.49%, 19.27%, 18.89% and 17.9%. The noted change of J_{SC} value with solar irradiance is mainly caused by the variation of the carrier's generation rate indicated in Fig. 12.

Fig.12 shows the expected result of carriers generating rate profile for the PSC as a function of the cell length, as the perovskite material has the smallest band gap among the PSC structure layers, then the incident light is absorbed in this main absorber layer causing carrier generating rate to reach its maximum value at the top edge of perovskite layer or at the interface between the active material and ETL, located at 583 nm in our proposed structure, and starts to decrease inside this layer until it reaches to 0 again at the interface between the perovskite material and the interface between the active material and HTL at 183nm.

Fig. 13 indicates the PSCs JV curve with different values of both temperature and solar irradiance. Variation of solar irradiance and temperature from 1000W/m^2, 30°C to 100W/m^2 and 80°C causes the value of JSC to drop by 90%, drop of V_{OC} by factor of 20.2%, and 4.86% PCE reduction.

D. EFFECT OF CHANGING ETL GEOMETRY

To study the effect of changing ETL geometric structure, the PSCs structure was modified with different shapes shown in Fig. 1(b), then optical study was recomputed to extract carriers generation rates then export them to electrical study to determine the electrical parameters of PSC for each case.

The maximum photogenerated carriers rate at the perovskite top edge interface with ETL was found to be $1.817*10^{28}m^{-3}s^{-1}$, $1.879*10^{28}m^{-3}s^{-1}$, $1.903*10^{28}$ $m^{-3}s^{-1}$, $1.944*10^{28}m^{-3}s^{-1}$ for flat, spherical, trapezoidal and pyramid shape respectively, which indicates higher carrier generating rate in case of pyramidal ETL by factor of 6.989% compared to the planar shape.

Electrical parameters of PSC resulting from changing ETL geometry were extracted from the JV curves shown in Fig. 14 and summarized in Table 2.

TABLE 2. Electrical parameters values of PSC with different ETL geometry.

Parameters	Flat ETL	Spherical ETL	Pyramidal ETL	Trapezoidal ETL
J_{SC} (mA/cm^2)	24.3658	25.5671	25.858	25.2439
V_{OC} $(Volt)$	0.99	1	1	1
J_{mp} (mA/cm^2)	23.3157	24.4898	24.7742	24.174
V_{mp} $(Volt)$	0.85	0.85	0.85	0.85
FF (%)	82.16	81.42	81.44	81.4
PCE (%)	19.818	20.8164	21.058	20.5479

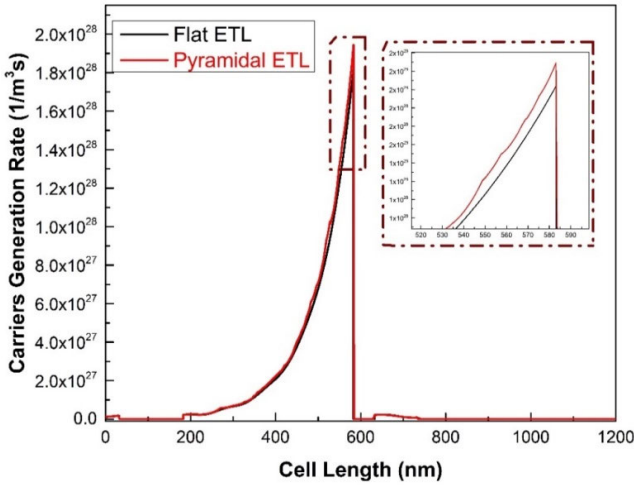

FIGURE 15. Generation rate of carriers for PSC with flat and pyramidal ETL geometries.

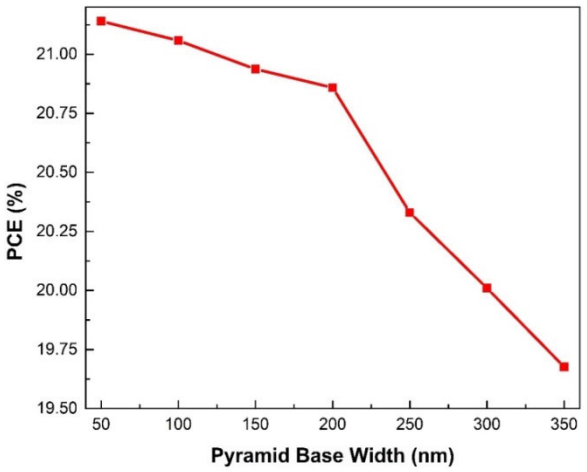

FIGURE 16. Effect of changing pyramid grating base width on the PCE of the cell.

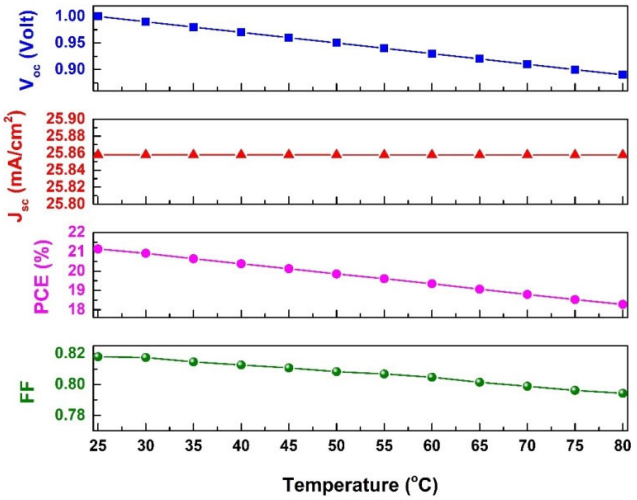

FIGURE 17. Pyramidal ETL PSC's parameters variation depending on temperature.

As indicated in Table 2 changing the shape of ETL mainly affects the short circuit current density, while, open circuit voltage is nearly not affected as there is neither energy level nor recombination rates changing.

The reason of such improving of J_{SC} in case of pyramidal geometry of ETL is the enhancement of the absorption and carriers photogeneration rates of the cell as pyramidical grating shapes have the ability of scattering more light into the main absorber than other geometries.

Fig. 15 indicates the enhancement of carriers' generation rates profile caused by changing the geometry of the ETL to pyramidal shape compared with the planar ETL structure which agrees with the previously mentioned results in Table 2.

Fig. 16 indicates the effect of base width variation of the pyramid grating on the PCE, showing reduction of the PCE with the increasing of base width. That comes as results of changing the capability of the scattering by variation of the scattering element dimension. Maximum PCE was found to be 21.058% with pyramid base width of 50nm.

Fig. 17 shows the effect of temperature variation on the pyramidal grated ETL PSC's parameters over 25 − 80°C temperature change range. Compared to results displayed in Fig. 7, results presented in Fig. 17 indicate that the reduction in PCE caused by temperature increasing can be compensated by changing the geometry of ETL to pyramidal shape.

IV. CONCLUSION

In this research article, a 3-D FEM numerical study has been introduced for PSC to investigate the electrical and optical effects of changing the thickness of both main absorber and carrier transporting layers, operating temperature and sun irradiance. Main parameters of the proposed PSC have been introduced by computing optical and electrical studies then getting the main parameters from JV curves in each case. Results have indicated that optimized thickness for each layer in our study are 400nm for the main absorber, 50nm for the ETL, 150nm for the HTL and 100nm for the front transparent conducting layer with corresponding maximum PCE value of 19.818% . Changing temperature mainly affects the value of open circuit voltage causing overall drop in PCE of 2.722% for temperature variation between 25 − 80°C. While solar

irradiance mainly affects the short circuit current, results have shown that changing temperature and solar power at the same time may cause degradation of PCE by 4.86%. Also, results have indicated that changing the geometric shape of ETL to pyramidal shape instead of flat shape can increase the PCE of PSC by 1.24% which can be utilized as a compensating technique of efficiency reduction caused by increased temperature.

REFERENCES

[1] P. P. Boix, K. Nonomura, N. Mathews, and S. G. Mhaisalkar, "Current progress and future perspectives for organic/inorganic perovskite solar cells," *Mater. Today*, vol. 17, no. 1, pp. 16–23, Feb. 2014, doi: 10.1016/j.mattod.2013.12.002.

[2] N. M. Ali, T. A. Ali, and N. H. Rafat, "A comparison between different structures of perovskite nanorod solar cells," *Optik*, vol. 202, Feb. 2020, Art. no. 163645, doi: 10.1016/j.ijleo.2019.163645.

[3] M. A. Green, A. Ho-Baillie, and H. J. Snaith, "The emergence of perovskite solar cells," *Nature Photon.*, vol. 8, no. 7, pp. 506–514, 2014, doi: 10.1038/nphoton.2014.134.

[4] A. A. Tabrizi, H. Saghaei, M. A. Mehranpour, and M. Jahangiri, "Enhancement of absorption and effectiveness of a perovskite thin-film solar cell embedded with gold nanospheres," *Plasmonics*, vol. 16, no. 3, pp. 747–760, Jun. 2021, doi: 10.1007/s11468-020-01341-1.

[5] J. Yan, T. J. Savenije, L. Mazzarella, and O. Isabella, "Progress and challenges on scaling up of perovskite solar cell technology," *Sustain. Energy Fuels*, vol. 6, no. 2, pp. 243–266, Jan. 2022, doi: 10.1039/d1se01045j.

[6] S. Rani, A. Kumar, and D. S. Ghosh, "Optical designing of perovskite solar cells," *IEEE J. Photovolt.*, vol. 12, no. 2, pp. 595–601, Mar. 2022, doi: 10.1109/JPHOTOV.2022.3141344.

[7] K. Akihiro, T. Kenjiro, S. Yasuo, and M. Tsutomu, "Organometal halide perovskites as visible-light sensitizers for photovoltaic cells," *J. Amer. Chem. Soc.*, vol. 131, no. 17, pp. 6050–6051, Apr. 2009, doi: 10.1021/ja809598r.

[8] J. Jeong et al., "Pseudo-halide anion engineering for α-$FAPbI_3$ perovskite solar cells," *Nature*, vol. 592, no. 7854, pp. 381–385 Apr. 2020.

[9] I. M. De Los Santos, H. J. Cortina-Marrero, M. A. Ruíz-Sánchez, L. Hechavarría-Difur, F. J. Sánchez-Rodríguez, M. Courel, and H. Hu, "Optimization of $CH_3NH_3PbI_3$ perovskite solar cells: A theoretical and experimental study," *Sol. Energy*, vol. 199, pp. 198–205, Mar. 2020, doi: 10.1016/j.solener.2020.02.026.

[10] R. Chang, Y. Yan, J. Zhang, Z. Zhu, and J. Gu, "Large-grain and smooth cesium doped $CH_3NH_3PbI_3$ perovskite films by cesium iodide post-treatment for improved solar cells," *Thin Solid Films*, vol. 712, Oct. 2020, Art. no. 138279, doi: 10.1016/j.tsf.2020.138279.

[11] F. S. Ghoreishi, V. Ahmadi, R. Poursalehi, M. SamadPour, M. B. Johansson, G. Boschloo, and E. M. J. Johansson, "Enhanced performance of $CH_3NH_3PbI_3$ perovskite solar cells via interface modification using phenyl ammonium iodide derivatives," *J. Power Sources*, vol. 473, Oct. 2020, Art. no. 228492, doi: 10.1016/j.jpowsour.2020.228492.

[12] P. Zhou, B. Li, Z. Fang, W. Zhou, M. Zhang, W. Hu, T. Chen, Z. Xiao, and S. Yang, "Nitrogen-doped nickel oxide as hole transport layer for high-efficiency inverted planar perovskite solar cells," *Sol. RRL*, vol. 3, no. 10, pp. 1–8, 2019, doi: 10.1002/solr.201900164.

[13] A. Babayigit, A. Ethirajan, M. Müller, and B. Conings, "Toxicity of organometal halide perovskite solar cells," *Nature Mater.*, vol. 15, no. 3, pp. 247–251, Mar. 2016, doi: 10.1038/nmat4572.

[14] H. Hu, B. Dong, and W. Zhang, "Low-toxic metal halide perovskites: Opportunities and future challenges," *J. Mater. Chem. A*, vol. 5, no. 23, pp. 11436–11449, 2017, doi: 10.1039/c7ta00269f.

[15] N. Thakur, S. Mishra, and P. Guha, "Performance analysis of transition metals embedded tin halide perovskite solar cell," *IEEE J. Photovolt.*, vol. 12, no. 3, pp. 728–736, May 2022, doi: 10.1109/JPHOTOV.2022.3144772.

[16] G. Faraone, R. Modi, S. Marom, A. Podestà, and M. Di Vece, "Increasing the optical absorption in a-Si thin films by embedding gold nanoparticles," *Opt. Mater.*, vol. 75, pp. 204–210, Jan. 2018, doi: 10.1016/j.optmat.2017.10.025.

[17] R. Irandoost and S. Soleimani-Amiri, "Design and analysis of high efficiency perovskite solar cell with ZnO nanorods and plasmonic nanoparticles," *Optik*, vol. 202, Feb. 2020, Art. no. 163598, doi: 10.1016/j.ijleo.2019.163598.

[18] S. Zhang, M. Liu, W. Liu, Y. Liu, Z. Li, X. Wang, and F. Yang, "Absorption enhancement in thin film solar cells with bilayer silver nanoparticle arrays," *J. Phys. Commun.*, vol. 2, no. 5, May 2018, Art. no. 055032, doi: 10.1088/2399-6528/aac41b.

[19] A. Tooghi, D. Fathi, and M. Eskandari, "Numerical study of a highly efficient light trapping nanostructure of perovskite solar cell on a textured silicon substrate," *Sci. Rep.*, vol. 10, no. 1, pp. 1–13, Oct. 2020, doi: 10.1038/s41598-020-75630-4.

[20] A. Razzaq, V. Depauw, H. S. Radhakrishnan, J. Cho, I. Gordon, J. Szlufcik, Y. Abdulraheem, and J. Poortmans, "Infrared absorption enhancement using periodic inverse nanopyramids in crystalline-silicon bottom cells for application in tandem devices," *IEEE J. Photovolt.*, vol. 10, no. 3, pp. 740–748, May 2020, doi: 10.1109/JPHOTOV.2020.2972324.

[21] J. Wu, "Absorption enhancement in thin-film solar cells based on periodically chirped structure," *Sol. Energy*, vol. 165, pp. 85–89, May 2018, doi: 10.1016/j.solener.2018.03.004.

[22] H. Zhang, M. Kramarenko, J. Osmond, J. Toudert, and J. Martorell, "Natural random nanotexturing of the Au interface for light backscattering enhanced performance in perovskite solar cells," *ACS Photon.*, vol. 5, no. 6, pp. 2243–2250, Jun. 2018, doi: 10.1021/acsphotonics.8b00099.

[23] R. Dewan, S. Shrestha, V. Jovanov, J. Hüpkes, K. Bittkau, and D. Knipp, "Random versus periodic: Determining light trapping of randomly textured thin film solar cells by the superposition of periodic surface textures," *Sol. Energy Mater. Sol. Cells*, vol. 143, pp. 183–189, Dec. 2015, doi: 10.1016/j.solmat.2015.06.014.

[24] M. K. Sahoo and P. Kale, "Integration of silicon nanowires in solar cell structure for efficiency enhancement: A review," *J. Materiomics*, vol. 5, no. 1, pp. 34–48, Mar. 2019, doi: 10.1016/j.jmat.2018.11.007.

[25] X. Yuan, X. Chen, X. Yan, W. Wei, Y. Zhang, and X. Zhang, "Absorption-enhanced ultra-thin solar cells based on horizontally aligned p-i-n nanowire arrays," *Nanomaterials*, vol. 10, no. 6, pp. 1–11, 2020, doi: 10.3390/nano10061111.

[26] V. Consonni, J. Briscoe, E. Kärber, X. Li, and T. Cossuet, "ZnO nanowires for solar cells: A comprehensive review," *Nanotechnology*, vol. 30, no. 36, Sep. 2019, Art. no. 362001, doi: 10.1088/1361-6528/ab1f2e.

[27] W. Liu, H. Ma, and A. Walsh, "Advance in photonic crystal solar cells," *Renew. Sustain. Energy Rev.*, vol. 116, Dec. 2019, Art. no. 109436, doi: 10.1016/j.rser.2019.109436.

[28] N. D. Gupta and V. Janyani, "Design and analysis of light trapping in thin film GaAs solar cells using 2-D photonic crystal structures at front surface," *IEEE J. Quantum Electron.*, vol. 53, no. 2, pp. 1–9, Apr. 2017, doi: 10.1109/JQE.2017.2667638.

[29] K. Ishizaki, M. De Zoysa, Y. Tanaka, S.-W. Jeon, and S. Noda, "Progress in thin-film silicon solar cells based on photonic-crystal structures," *Jpn. J. Appl. Phys.*, vol. 57, no. 6, Jun. 2018, Art. no. 060101, doi: 10.7567/JJAP.57.060101.

[30] H. Talebi and F. Emami, "Design of ultrathin hole-transport-layer-free perovskite solar cell with near-infrared absorption enhancement using Ag NPs," *Opt. Commun.*, vol. 520, Oct. 2022, Art. no. 128553, doi: 10.1016/j.optcom.2022.128553.

[31] L. Lin, L. Jiang, P. Li, D. Chen, Z. Kang, H. Xiong, Q. Yan, X. Lin, and Y. Qiu, "Broadband absorption enhancement in carbon-based perovskite solar cell with a composite light trapping structure," *Micro Nanostruct.*, vol. 166, Jun. 2022, Art. no. 207227, doi: 10.1016/j.micrna.2022.207227.

[32] N. D. Pham, A. Singh, W. Chen, M. T. Hoang, Y. Yang, X. Wang, A. Wolff, X. Wen, B. Jia, P. Sonar, and H. Wang, "Self-assembled carbon dot-wrapped perovskites enable light trapping and defect passivation for efficient and stable perovskite solar cells," *J. Mater. Chem. A*, vol. 9, no. 12, pp. 7508–7521, Mar. 2021, doi: 10.1039/d1ta00036e.

[33] M. H. Mohammadi, D. Fathi, and M. Eskandari, "Light trapping in perovskite solar cells with plasmonic core/shell nanorod array: A numerical study," *Energy Rep.*, vol. 7, pp. 1404–1415, Nov. 2021, doi: 10.1016/j.egyr.2021.02.071.

[34] M. Alla, V. Manjunath, N. Chawki, D. Singh, S. C. Yadav, M. Rouchdi, and F. Boubker, "Optimized $ch_3nh_3pbi_{3-x}cl_x$ based perovskite solar cell with theoretical efficiency exceeding 30%," *Opt. Mater.*, vol. 124, Feb. 2022, Art. no. 112044, doi: 10.1016/j.optmat.2022.112044.

[35] P. Saxena and N. E. Gorji, "COMSOL simulation of heat distribution in perovskite solar cells: Coupled optical–electrical–thermal 3-D analysis," *IEEE J. Photovolt.*, vol. 9, no. 6, pp. 1693–1698, Nov. 2019, doi: 10.1109/JPHOTOV.2019.2940886.
[36] S. Zandi and M. Razaghi, "Finite element simulation of perovskite solar cell: A study on efficiency improvement based on structural and material modification," *Sol. Energy*, vol. 179, pp. 298–306, Feb. 2019, doi: 10.1016/j.solener.2018.12.032.
[37] T. Minemoto and M. Murata, "Device modeling of perovskite solar cells based on structural similarity with thin film inorganic semiconductor solar cells," *J. Appl. Phys.*, vol. 116, no. 5, pp. 2–8, 2014, doi: 10.1063/1.4891982.
[38] F. Jahantigh and S. M. B. Ghorashi, "Optical simulation and investigation of the effect of hysteresis on the perovskite solar cells," *Nano*, vol. 14, no. 10, 2019, Art. no. 1950127, doi: 10.1142/S1793292019501273.
[39] E. Raoult, R. Bodeux, S. Jutteau, and S. Rives, "Optical characterizations and modelling of semitransparent perovskite solar cells for tandem applications," in *Proc. 36th Eur. Photovoltaic Solar Energy Conf. Exhib.*, vol. 36, 2019, pp. 757–763, doi: 10.4229/EUPVSEC20192019-3BV.2.53.
[40] S. Manzoor, J. Häusele, K. A. Bush, A. F. Palmstrom, J. Carpenter, Z. J. Yu, S. F. Bent, M. D. Mcgehee, and Z. C. Holman, "Optical modeling of wide-bandgap perovskite and perovskite/silicon tandem solar cells using complex refractive indices for arbitrary-bandgap perovskite absorbers," *Opt. Exp.*, vol. 26, no. 21, p. 27441, Oct. 2018, doi: 10.1364/oe.26.027441.
[41] V. Mishra, M. K. Warshi, A. Sati, A. Kumar, V. Mishra, R. Kumar, and P. R. Sagdeo, "Investigation of temperature-dependent optical properties of TiO_2 using diffuse reflectance spectroscopy," *Social Netw. Appl. Sci.*, vol. 1, no. 3, pp. 1–8, Mar. 2019, doi: 10.1007/s42452-019-0253-6.
[42] B. J. Foley, D. L. Marlowe, K. Sun, W. A. Saidi, L. Scudiero, M. C. Gupta, and J. J. Choi, "Temperature dependent energy levels of methylammonium lead iodide perovskite," *Appl. Phys. Lett.*, vol. 106, no. 24, pp. 581–586, Aug. 2015, doi: 10.1063/1.4922804.
[43] Y. Cho, A. Yamaguchi, R. Uehara, S. Yasuhara, T. Hoshina, and M. Miyauchi, "Temperature dependence on bandgap of semiconductor photocatalysts," *J. Chem. Phys.*, vol. 152, no. 23, Jun. 2020, Art. no. 231101, doi: 10.1063/5.0012330.
[44] C. Q. Xia, J. Peng, S. Poncé, J. B. Patel, A. D. Wright, T. W. Crothers, M. U. Rothmann, J. Borchert, R. L. Milot, H. Kraus, Q. Lin, F. Giustino, L. M. Herz, and M. B. Johnston, "Limits to electrical mobility in lead-halide perovskite semiconductors," *J. Phys. Chem. Lett.*, vol. 12, no. 14, pp. 3607–3617, Apr. 2021, doi: 10.1021/acs.jpclett.1c00619.
[45] R. V. Krishna, B. Mahapatra, and P. K. Patel, "Effect of electrical parameters on lead-based perovskite solar cell for high-efficiency performance," *Opt. Quantum Electron.*, vol. 54, no. 8, pp. 1–12, Aug. 2022, doi: 10.1007/s11082-022-03738-0.

ALAA A. ZAKY received the B.Sc. degree in electrical power and machines engineering from Kafrelsheikh University, Egypt, in 2007, the M.Sc. degree in electrical power and machines engineering from Mansoura University, Egypt, in 2015, and the Ph.D. degree in electrical engineering from the School of Electrical and Computer Engineering, National Technical University of Athens, in 2021. In 2008, he became a Teaching Staff with the Electrical Engineering Department, Kafrelsheikh University, where he has been an Assistant Professor with the Department of Electrical Engineering, since 2021. His current research interests include renewable energy, solar energy technologies, third-generation solar cells, optimization, and power system operation and control. He received the Kafrelsheikh University Award for his international scientific publications (several times).

SHOROK ELEWA received the B.Sc. degree in electrical engineering from Kafrelsheikh University, Kafrelsheikh, Egypt, in 2016, and the M.Sc. degree in electronics and electrical communications engineering from Mansoura University, Egypt, in 2022. She is an Assistant Lecturer with the Electronics and Communications Engineering Branch, Electrical Engineering Department, Faculty of Engineering, Kafrelsheikh University. Her research and teaching interests include modeling of electromagnetic and photonic devices and nano-electronics and solar energy systems modeling, design, and simulation.

SALEH ALYAHYA (Member, IEEE) received the bachelor's degree in engineering in communications engineering from the University of Portsmouth, U.K., in 2010, the M.Sc. degree in technology management from the School of Engineering, University of Portsmouth, in 2011, and the Ph.D. degree in engineering from the School of Engineering, University of Portsmouth. His research thesis was titled "Integration and Optimization of an RFID-Enabled Inventory Management System of a Future Generation Warehousing System." His M.Sc. research dissertation was titled "A Novel Design of a Manual Assembly System Incorporating Walking Workers." He is currently the Deputy Dean of Academics with the College of Engineering and Information Technology, Onaizah Colleges, Al Qassim, Saudi Arabia. His research interests include RFID, the IoT, and network security. He received a final-year research title as a Digital Speech Recorder. He is the IEEE Pattern for Onaizah College of Engineering and Information Technology. Regarding the research contribution, during his Ph.D. (four years) study, he gave significant assistance in supervising students' projects and assessing students' presentations at many teaching sessions.

MUJAHED AL-DHAIFALLAH (Member, IEEE) received the B.Sc. and M.Sc. degrees in systems engineering from the King Fahd University of Petroleum and Minerals, Dhahran, Saudi Arabia, and the Ph.D. degree in electrical and computer engineering from the University of Calgary, Calgary, AB, Canada. Since 2020, he has been an Associate Professor of control and instrumentation engineering with the King Fahd University of Petroleum and Minerals. His current research interests include nonlinear systems identification, control systems, optimization, artificial intelligence, and renewable energy.

HEGAZY REZK is the Chairperson of the Department of Electrical Engineering, College of Engineering in Wadi Alddawasir, Prince Sattam Bin Abdulaziz University, Saudi Arabia. His current research interests include renewable energy, smart grids, hybrid systems, optimization, and artificial intelligence.

BEDIR YOUSIF (Member, IEEE) received the B.Sc. degree in electronics engineering from the Faculty of Electronic Engineering, Menoufia University, Egypt, in 1999, and the master's and Ph.D. degrees from the Electronics and Communications Department, Faculty of Engineering, Mansoura University, Egypt, in 2006 and 2013, respectively. He is an Associate Professor with the Electronics and Communications Engineering Branch, Electrical Engineering Department, Faculty of Engineering, Kafrelsheikh University; and the Head of the Electrical Engineering Department, Faculty of Engineering and Information Technology, Onaizah Colleges, Al Qassim, Saudi Arabia. He has several publications in the modeling of plasmonic devices, photovoltaics energy systems, and optical communications. His research and teaching interests include modeling of electromagnetic and photonic devices, nano-electronics, and optical communications.